Affine Invariant Shape Matching using Histogram of Radon Transform and Angle Correlation Matrix

Makoto Hasegawa[1] and Salvatore Tabbone[2]
[1]*Tokyo Denki University, 5 Senju Asahi-cho, Adachi-ku, Tokyo 120-8551 Japan*
[2]*LORIA, UMR 7503, Université de Lorraine, 54506 Vandoeuvre-lès-Nancy, France*

Keywords: Shape Descriptor, Affine Invariance, Radon Transform, Dynamic Time Warping Distance, Beam Search.

Abstract: An affine invariant shape matching descriptor using the histogram of Radon transform (HRT) and the dynamic time warping (DTW) distance is proposed. Our descriptor based on the Radon transform is robust to shape rotation, uniform scaling, and translation. For non-uniform scaling and shearing, our descriptor has a non-linear sparse and dense distortion relative to the angle coordinates. Therefore, we apply DTW on a cost matrix to be robust to these transformations. This cost matrix is defined as an angle correlation matrix based on the product of two matrices only. Moreover, based on the beam search algorithm, we speed-up the time complexity of our method. Experimental results show that our approach is fast to compute and competitive compared to well-known descriptors.

1 INTRODUCTION

Geometric invariant shape descriptors are very important for shape recognition. Usually shape descriptors need to be invariant to classical geometric transformations like rotation, scaling and translation. However these transformations are not enough in several applications. Recently, a shape recognition application using a portable digital camera has been proposed in (Liang et al., 2005) where shapes (included in the photos) are deformed following affine distortions. Therefore, it is necessary to be invariant to such distortions.

RST invariant descriptors have been proposed for shapes description and matching. Fourier transform has been used as the starting point for the proposal of many shape descriptors. The generic Fourier descriptor (GFD) proposed by D. Zhang and G. Lu (Zhang and Lu, 2002) is a typical one, and it is invariant to rotation. However, in the case of translation and scaling, GFD needs normalizations. The phase-only correlation function (POC) proposed by C. Kuglin et al. (D., 1975) has been shown to be effective for shape matching. The Fourier–Mellin transform (FMT) proposed by Chen et al. (Chen et al., 1994) is a typical Fourier descriptor invariant to RST transformations. Fourier descriptors have proved their robustness to RST transformations and many applications have been developed using these descriptors (Arafat et al., 2009; Yuyama and Mitsuhashi, 2008; Ouyang et al., 2006).

Many shape descriptors using the Radon transform (Deans, 1993) have been defined in the literature by Tabbone et al. (Tabbone et al., 2006). A method called the histogram of Radon transform (HRT) (Tabbone et al., 2008) has been proposed using the Radon transform and a two-dimensional histogram. This descriptor encodes the shape length at each orientation; it is invariant to the shape scaling and translation, and the shape rotation is projected to a horizontal translation on the domain. Recently, the Amplitude-only log Radon transform (ALR) (Hasegawa and Tabbone, 2012) has been defined. This descriptor is based on the Radon transform, amplitude extraction, and log mapping. It is invariant to shape translation; shape rotation and scaling are projected into a two-dimensional translation. To keep the invariance to these transformations (rotation and scaling) the phase-only correlation function is used where the computation of several Fourier transforms are needed. Combined with the DTW, this descriptor is in addition invariant to any affine distortions. The reported results on recognition rates are very good compared to the literature but the complexity of the approach is very high. A method proposed by K.C. et al. (Santosh et al., 2011) combined the Radon transform and the dynamic time warping. The authors apply directly the dynamic time warping to

Hasegawa M. and Tabbone S..
Affine Invariant Shape Matching using Histogram of Radon Transform and Angle Correlation Matrix.
DOI: 10.5220/0004787000210029
In *Proceedings of the 3rd International Conference on Pattern Recognition Applications and Methods* (ICPRAM-2014), pages 21-29
ISBN: 978-989-758-018-5

the radial coordinate in the Radon domain. The approach is invariant to the RST transformations also. In the case of invariant methods to any affine distortions, the local descriptor ASIFT was proposed by Morel and Yu (Morel and Yu, 2009). ASIFT is an enhanced method of the conventional SIFT proposed by Lowe (Lowe, 2004). Shape matching is performed following local features detected into the images.

In this paper, we focus on a novel shape matching and descriptor method robust to classical RST (Rotation Scaling Translation) transformations and to distortions especially for non-uniform scaling and shearing. We propose a new method based on HRT (Tabbone et al., 2008) . When a shape has any non-linear transformations as shearing or non-uniform scaling, we show that such non-linear shape transformations become an only horizontal sparse and dense distortion relative to the angular coordinates in the HRT domain. In order to obtain invariance to such horizontal distortions, we apply the DTW which is one of the famous method for non-linear matching. Our method is robust to not only RST transformations (rotation, scaling, and translation), but also non-linear shape transformations. Furthermore, a fast computation method with the beam search algorithm (Tillmann et al., 1997) is performed in our DTW. Our previous method with ALR-DTW descriptor needs the phase-only correlation to generate the angle correlation matrix. Our new method with HRT can generate the angle correlation matrix by a matrix product only, so we provide a very fast computation.

The remainder of this paper is organized as follows. The Radon transform and the HRT descriptor are recalled in Sections 2 and 3. Our shape matching methods – including the descriptor matching, the dynamic time warping method, and the beam search method are discussed in Section 4. Experimental results are given in Section 5, and finally our conclusions are drawn in Section 6.

2 RADON TRANSFORM

We recall the Radon transform definition in this section. Let a coordinate (x,y) in the two-dimensional $x-y$ plane described as $\mathbf{x}$, and an original image represented as $f(\mathbf{x})$. The Radon transform of $f(\mathbf{x})$ is defined as:

$$\mathcal{R}_f(\theta,\rho) = \int f(\mathbf{x})\delta(\mathbf{x}\cdot\xi-\rho)\mathrm{d}\mathbf{x}, \qquad (1)$$

where $\xi = (\cos\theta, \sin\theta)$, and $\delta(\cdot)$ is a delta function. In other words, the Radon transform is the integral of $f(\mathbf{x})$ over lines

$$L_{\theta\rho} = \{\mathbf{x} \in R^2 | \mathbf{x}\cdot\xi = \rho\}, \qquad (2)$$

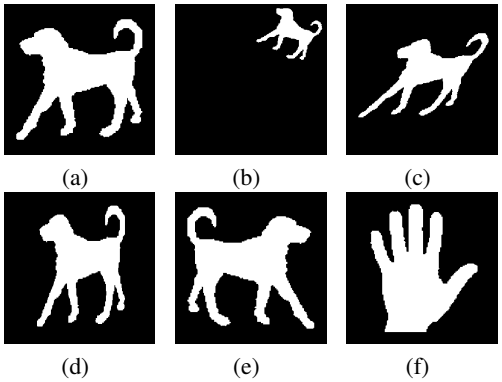

Figure 1: (a) Original image "Dog". (b) RST transformation. (c) Shearing. (d) Non-uniform scaling. (e) Reflection. (f) Original image "Hand".

where ρ is the distance between the origin and $L_{\theta\rho}$, the unit vector ξ and the angle θ describe the orientation of the line $L_{\theta\rho}$. The line integral is computed by a delta function $\delta(\cdot)$.

The Radon transform has useful properties for the RST transformations.

P1 *Rotation* : when shapes are rotated by θ_0, the Radon transform $\mathcal{R}_f(\theta,\rho)$ is translated to θ_0 relative to the coordinate θ as:

$$\mathcal{R}_f(\theta,\rho) \rightarrow \mathcal{R}_f(\theta-\theta_0,\rho), \qquad (3)$$

where $\mathcal{R}_f(\theta,\rho)$ is cyclic for θ as:

$$\mathcal{R}_f(-\theta,\rho) = \mathcal{R}_f(\pi-\theta,\rho). \qquad (4)$$

P2 *Scaling* : when shapes are scaled by α, the Radon transform $\mathcal{R}_f(\theta,\rho)$ is scaled by α relative to the coordinate ρ. Moreover, the magnitude of $\mathcal{R}_f(\theta,\rho)$ is multiplied by α as:

$$\mathcal{R}_f(\theta,\rho) \rightarrow \alpha\mathcal{R}_f\left(\theta,\frac{\rho}{\alpha}\right). \qquad (5)$$

P3 *Translation* : when shapes are translated to $\mathbf{x}_0$, the Radon transform $\mathcal{R}_f(\theta,\rho)$ is translated to $\mathbf{x}_0\cdot\xi$ relative to the coordinate ρ as:

$$\mathcal{R}_f(\theta,\rho) \rightarrow \mathcal{R}_f(\theta,\rho-\mathbf{x}_0\cdot\xi). \qquad (6)$$

The results of the Radon transform of Fig. 1 are shown in Fig. 2.

3 HISTOGRAM OF RADON TRANSFORM

3.1 Histogram

Let be f be a real function defined on a domain X : $f : X \rightarrow Y$. Besides, let us denote by # the cardinality

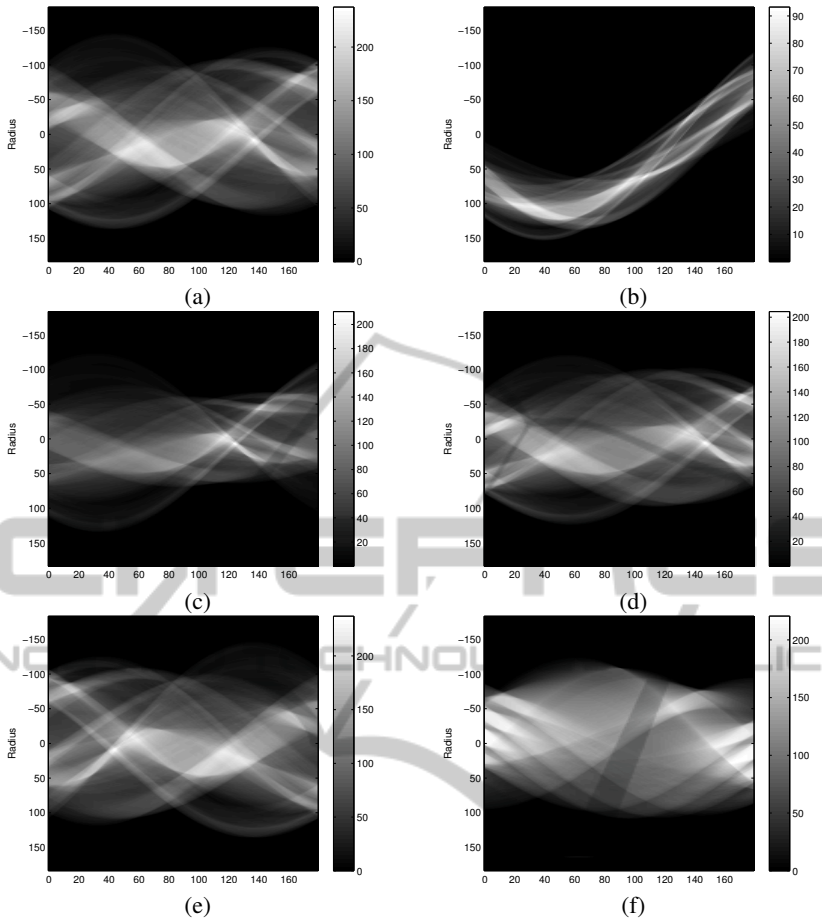

Figure 2: The Radon transform of Figs. 1(a) – 1(f).

of a set and by $|X|$ the size (length) of a domain X. Hence, the point-wise histogram of f is expressed by:

$$\mathcal{H}(f)(v) = \frac{\#\{x \in X | v = f(x)\}}{|X|}. \quad (7)$$

By the normalization using $|X|$ in Eq. (7), the histogram $\mathcal{H}(f)(v)$ means a generation probability of v.

Actually, the range of v is quantized by N bins v_i $(1 \leq i \leq N)$ and, we put the data $f(x)$ into the bins:

$$\mathcal{H}(f)(v_i) = \frac{\#\{x \in X | \ |f(x) - v_i| < \frac{\triangle}{2}\}}{|X|}, \quad (8)$$

where $\#\{.\}$ means the number of items in a bin, and:

$$\triangle = \frac{\max f(x) - \min f(x)}{N}. \quad (9)$$

The number of bins N is usually set by experience.

3.2 HRT Descriptor

The HRT descriptor is defined as a matrix of frequencies computed on the Radon transform for the angle parameter (Tabbone et al., 2008). Thus, the HRT descriptor represents a 2D histogram of shape lengths at each orientation. More precisely, the HRT descriptor $\mathcal{D}_f$ is:

$$\mathcal{D}_f(\theta, v) = \mathcal{H}(\mathcal{R}_f(\theta, \cdot))(v), \quad (10)$$

with

$$\mathcal{R}_f(\theta, \rho) \rightarrow \frac{\mathcal{R}_f(\theta, \rho)}{\max_{\theta,\rho}(\mathcal{R}_f(\theta, \rho))}, \quad (11)$$

where $\theta \in [0, \pi)$; $v > 0$, and X in Eq. (7) is:

$$X_\theta = \{\rho | \mathcal{R}_f(\theta, \rho) > 0\} \quad (12)$$

so that the generation probability of histograms is invariant to the shape scaling.

The HRT descriptor has beneficial properties as:

P4 *Rotation:* when shapes are rotated by θ_0, the HRT descriptor is translated to θ_0 relative to the coordinate θ as:

$$\mathcal{D}_f(\theta, v) \rightarrow \mathcal{D}_f(\theta - \theta_0, v), \quad (13)$$

where $\mathcal{D}(\theta, v)$ is cyclic for the θ as:

$$\mathcal{D}_f(-\theta, v) = \mathcal{D}_f(\pi - \theta, v). \quad (14)$$

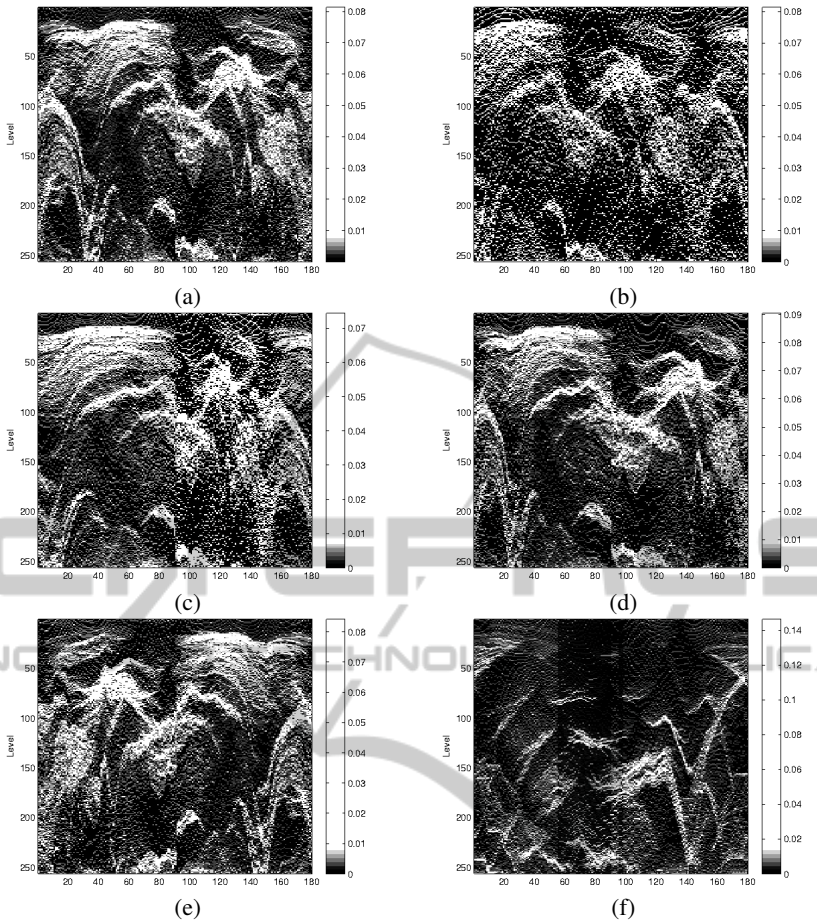

Figure 3: Our HRT for Figs. 1(a) – 1(f).

P5 *Scaling and Translation:* when shapes are scaled or translated, the HRT descriptor is invariant.

P6 *Non-linear Distortion:* when shapes get non-linear distortions as shearing or non-uniform scaling, the HRT descriptor gets sparse and dense distortion, only horizontally, on the transform domain.

Let's consider for instance Fig. 1(c). This figure is a slanted version ($\theta = 30^\circ$) of Fig. 1(a). Following the Radon transform, the integral of $f(\mathbf{x})$ over vertical lines ($\theta = 90^\circ$) on Fig. 1(a) are equal to the case of Fig. 1(c). On the other hand, the integral of $f(\mathbf{x})$ over horizontal lines ($\theta = 0^\circ$) on Fig. 1(a) are different from the slant lines on Fig. 1(c). As a result, some columns on the domain remain the same and some columns are translated horizontally. This result makes the horizontal sparse and dense distortion on the domain. Therefore, in order to obtain invariance to non-linear horizontal distortions, we apply the DTW for the non-linear matching.

The HRT descriptors of the original shapes in

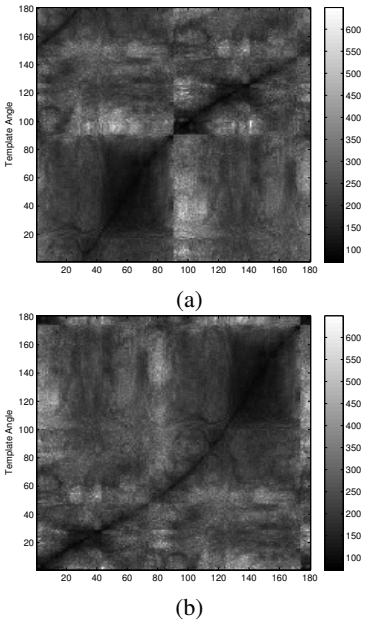

Figure 4: (a) The cost matrix for the HRT images shown in Figs. 3(a) and 3(c). (b) The normalized warping path.

Figs. 1(a)–1(f) are shown in Fig. 3 (where the number of bins $N = 256$). In the case of the RST transformations shown in Fig. 1(b), our descriptor shown in Fig. 3(b) is only translated horizontally for the shape rotation. Our descriptor is invariant to the shape scaling and translation. In the case of shearing and non-uniform scaling as shown in Figs. 1(c) and 1(d), our descriptor (see Figs. 3(c) and 3(d)) has horizontal sparse and dense distortions. In the case of reflection shown in Fig. 1(e), our descriptor (see Fig. 3(e)) is reflected in the angle coordinate. For a different shape shown in Fig. 1(f), our descriptor in Fig. 3(f) is different from Fig. 3(a).

4 SHAPE MATCHING

4.1 Angle Correlation Matrix

Since our descriptor is computed with discrete values, it can be described using a matrix as:

$$\mathcal{D}_f(\theta, v) \rightarrow \mathbf{D}_{\theta,v}, \tag{15}$$

where θ is digitized with integers $1 \sim 180$, and v is the bin number. Therefore, the size of $\mathbf{D}_{\theta,v}$ is $180 \times N$. Two descriptors one for the query and the other for the template are denoted as $\mathbf{Q}_{\theta,v}$ and $\mathbf{T}_{\theta,v}$.

Our angle correlation matrix $\mathbf{M}_{i,j}$ is computed as:

$$\mathbf{M}_{i,j} = \mathbf{Q}^{\mathrm{T}}_{j,v} \times \mathbf{T}_{i,v}, \tag{16}$$

where i and j are respectively the template and the query angle; the size of $\mathbf{M}_{i,j}$ is 180×180. $\mathbf{Q}^{\mathrm{T}}$ means a transposition of a matrix $\mathbf{Q}$. A cost matrix $\mathbf{C}_{i,j}$ is computed using the angle correlation matrix $\mathbf{M}_{i,j}$ as:

$$\mathbf{C}_{i,j} = \frac{1}{\mathbf{M}_{i,j}}. \tag{17}$$

A cost matrix $\mathbf{C}_{i,j}$ is shown in Fig. 4(a). A valley line (in black in the figure) called "warping path" appears in $\mathbf{C}_{i,j}$, when the two shapes are same even if they have RST transformations or any affine distortions.

The warping path is denoted as:

$$\mathbf{P} = \mathbf{p}_1, \mathbf{p}_2, \cdots, \mathbf{p}_k, \cdots, \mathbf{p}_K, \tag{18}$$

where $\mathbf{p}_k$ is a coordinate (i_k, j_k) on $\mathbf{C}_{i,j}$, $\mathbf{p}_1 = (1,1)$, $\mathbf{p}_K = (180,180)$, and $180 \leq K < 360$. We normalize $\mathbf{C}_{i,j}$ periodically so that the position with the minimum value in $\mathbf{C}_{i,j}$ becomes $(1,1)$. If the minimum value in $\mathbf{C}_{i,j}$ is not unique, the minimum value on the most upper-left on the image is chosen. Fig. 4(b) is the result of the normalized warping path.

Cost matrices shown in Figs. 5(a) – 5(e) are cases using the query shown in Fig. 3(a) and templates shown in Figs. 3(b) – 3(f), respectively. For only RST transformations (see Fig. 5(a)), a straight valley line appears in the domain. In the case of shearing and non-uniform scaling shown in Figs. 5(b) and 5(c), a curved valley line appears in each case. A cost matrix for shapes which are different as shown in Fig. 5(e) has no valley line.

In the case of the shape reflection, the Radon image and HRT image are reflected following the angular coordinate as shown in Figs. 2(e) and 3(e). Since the corresponding angle order is reversed, the cost matrix $\mathbf{C}_{i,j}$ is set as: $\mathbf{C}_{i,j} \leftarrow \mathbf{C}_{i,181-j}$. In this case, the cost matrix show (see Fig. 5(d)) a straight valley line with negative slope due to the reflection property of the Radon transform.

4.2 Dynamic Time Warping (DTW)

Our dynamic time warping is performed using an accumulated cost matrix $\mathbf{A}_{i,j}$ to search the minimum cost as:

$$\mathbf{A}_{i,j} = \mathbf{C}_{i,j} + \min_{(m,n)} \mathbf{A}_{m,n}$$
$$(m,n) \in \{(i-1,j),(i,j-1),(i-1,j-1)\}, \tag{19}$$

where $\mathbf{A}_{1,j} = \mathbf{C}_{1,j} + \mathbf{A}_{1,j-1}$; $\mathbf{A}_{i,1} = \mathbf{C}_{i,1} + \mathbf{A}_{i-1,1}$; $\mathbf{A}_{1,1} = \mathbf{C}_{1,1}$. Therefore, Eq. (19) tracks the warping path. An accumulated cost matrix $\mathbf{A}_{i,j}$ is shown in Fig. 6.

We track back the warping path $\mathbf{p}_k = (i_k, j_k)$ from $\mathbf{p}_K = (180,180)$ to $\mathbf{p}_0 = (1,1)$ as:

$$\mathbf{p}_{k-1} = \arg\min_{(m,n)} \mathbf{A}_{m,n}$$
$$(m,n) \in \{(i_k-1, j_k),(i_k, j_k-1),(i_k-1, j_k-1)\}. \tag{20}$$

The matching score between two shapes is computed using the path length K as:

$$S = \frac{K}{\mathbf{A}_{180,180}}. \tag{21}$$

Warping paths shown in Figs. 7(a) – 7(e) are the case using a query shown in Fig. 3(a) and templates shown in Figs. 3(b) – 3(f), respectively. A warping path under the RST transformations shown in Fig. 7(a) is a straight line. In the case of shearing and non-uniform scaling shown in Figs. 7(b) and 7(c), their warping paths are curved lines. In the case of reflection and matching with different shapes (see Figs. 7(d) and 7(e)), their corresponding warping paths are also straight lines.

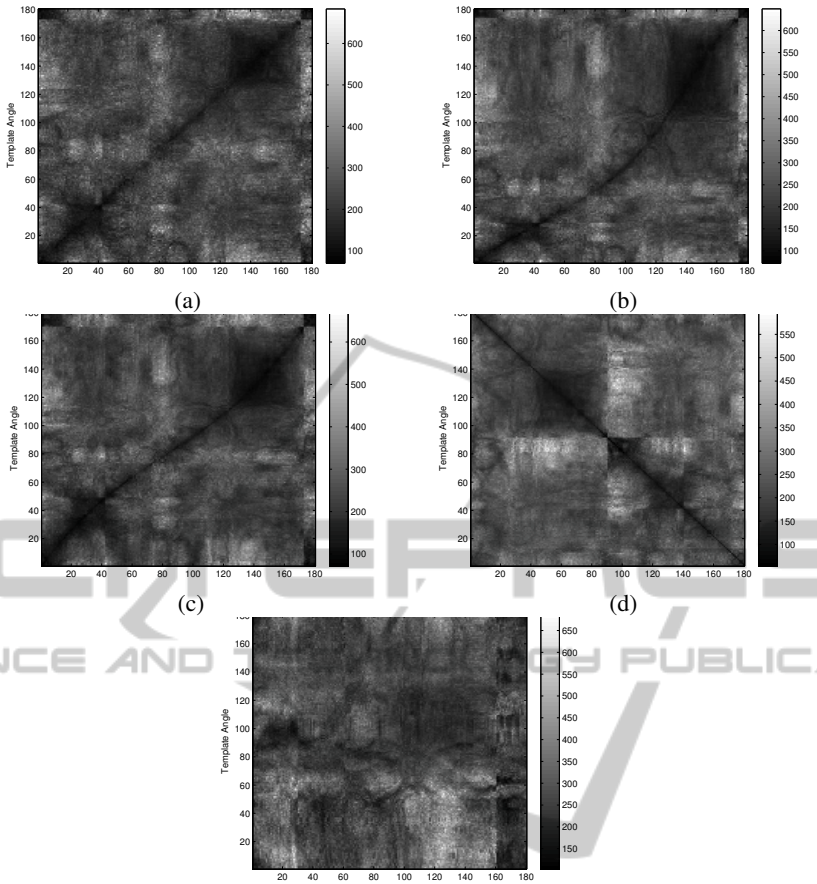

Figure 5: Cost matrices: (a) – (e) are the cases with a query shown in Fig. 3(a) and templates shown in Figs. 3(b) – 3(f), respectively.

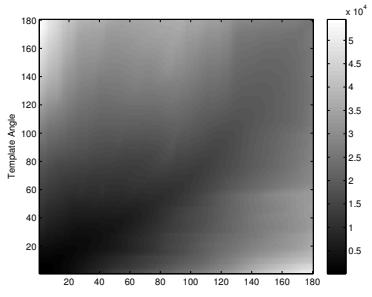

Figure 6: The accumulated cost matrix of Fig. 4(b).

4.3 Beam Search

The beam search(Tillmann et al., 1997) is a fast computation algorithm for the DTW. Our beam search skips $\mathbf{A}_{i,j}$ computation in Eq. (19), when $\mathbf{A}_{i-1,j} > T_{i-1,j}$, $\mathbf{A}_{i,j-1} > T_{i,j-1}$, and $\mathbf{A}_{i-1,j-1} > T_{i-1,j-1}$ ($\mathbf{A}_{i,j}$ is initialized to ∞ at the first), where:

$$T_{i,j} = T_{min} + (T_{max} - T_{min}) \times \frac{i+j}{360}. \qquad (22)$$

T_{min} and T_{max} are thresholds for the beam band. It means a pruning searching tree defined by Eq. (19).

An accumulated cost matrix without the beam search is shown in Fig. 8(a). Its warping paths is denoted using a black line. The result of the beam search, an accumulated cost matrix within thresholds $T_{min} = 1000$ and $T_{max} = 30000$ is shown in Fig. 8(b). A search band is generated, and the computation for the accumulated cost matrix is reduced. We can remark that the warping path is included in the search band.

5 EXPERIMENTAL RESULTS

To demonstrate the performance of our descriptor, we have carried out experiments based on commonly used binary datasets. An affine distorted shape dataset

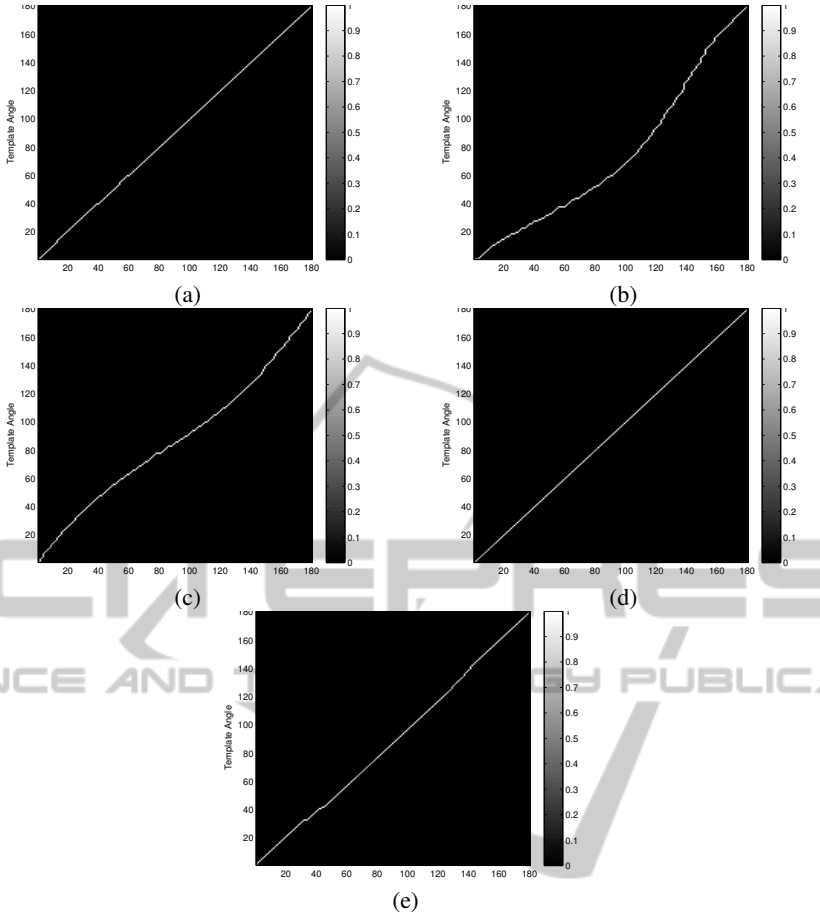

Figure 7: Warping paths: (a) – (e) are the cases with a query shown in Fig. 3(a) and templates shown in Figs. 3(b) – 3(f), respectively.

shown in Fig. 9 consists of 9 categories with affine distortions (99 images). These datasets are created from a commonly used dataset in many works and is available from the research community[1].

Our method (HRT-DTW) is computed with and without the beam search algorithm; ALR with the dynamic time warping (ALR-DTW) (Hasegawa and Tabbone, 2012), HRT (Tabbone et al., 2008), FMT (Chen et al., 1994), and ASIFT (Morel and Yu, 2009). In the case of ASIFT, we use an source code provided by Morel and Yu on their web site [2].

The performance is evaluated using the precision-recall measure (Davis and Goadrich, 2006) defined as:

$$\text{Precision} = \frac{tp}{tp+fp}$$
$$\text{Recall} = \frac{tp}{tp+fn}, \qquad (23)$$

where the true positives tp is the number of items correctly labeled as belonging to the positive class, the false positives fp is the number of items incorrectly labeled as belonging to the class, and the false negatives fn is the number of items which were not labeled as belonging to the positive class but should have been. Namely, the precision is the number of true positives divided by the total number of elements labeled as belonging to the positive class. The recall is the number of true positive divided by the total number of elements that actually belong to the positive class. We create a precision-recall curve by plotting Precision and Recall at each retrieval rate.

Precision-recall curves of each method is shown in Fig. 10. Our method and ALR-DTW are very similar and have very high performances compared to the other. Both descriptors are robust to any affine distortions. Moreover, we can remark no decrease with the beam search algorithm.

The processing time to match two images for different methods is shown in Table 1 using Intel Core

[1]http://www.lems.brown.edu/vision/researchAreas/SIID/
[2]http://www.cmap.polytechnique.fr/ yu/

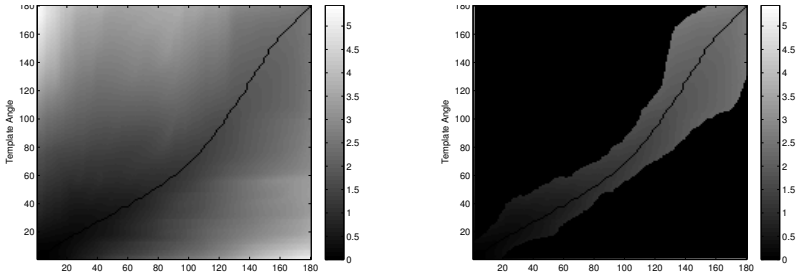

(a) (b)

Figure 8: (a) The accumulated cost matrix; (b) the result of the beam search with the thresholds $T_{min} = 1000$ and $T_{max} = 30000$. The warping paths are denoted with black lines.

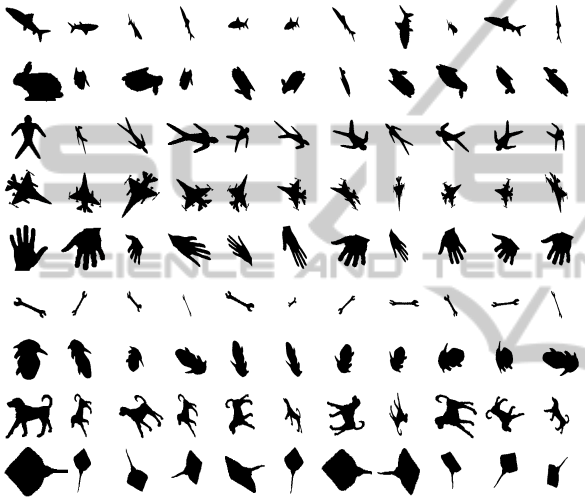

Figure 9: An affine distorted dataset. This dataset has 9 categories with affine distortions.

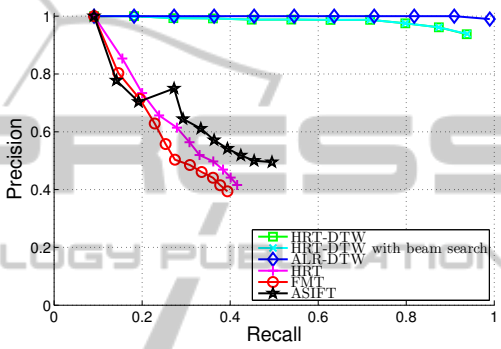

Figure 10: Precision-recall curves of each method.

Table 1: Processing time for the matching between two images.

Method	Time [Sec.]
HRT-DTW	0.43
HRT-DTW(with beam search)	0.27
ALR-DTW	4.03
HRT	0.01
FMT	0.01
ASIFT	11.97

i7-366U 2.00 GHz CPU. ASIFT is implemented in C, and the other methods are implemented using MATLAB. HRT and FMT are very fast, however they are not robust to any affine distortions. Comparing with ALR-DTW, our processing time is about one tenth compared to ALR-DTW. It is observed that the computing of the angle correlation matrix by a matrix product in Eq. (16) provides very fast computation and the processing time using our beam search algorithm is significant (about one half less time compared to HRT-DTW).

6 CONCLUSIONS

We propose a new method based on the HRT descriptor. The HRT descriptor is robust to shape scaling, translation and rotation. However, for non-uniform shape scaling and shearing, this descriptor has a nonlinear sparse and dense distortions relative to the angle coordinates. Therefore, we propose a novel affine invariant shape matching combining HRT with the DTW. DTW is set on a cost matrix defined as an angle correlation matrix based on the product of two matrices only. The computational complexity is reduced using the beam search algorithm. Reported results on a common dataset have shown a very good robustness to any affine transformations with low complexity time thanks to the angle correlation matrix product and the beam search algorithm.

In order to keep our approach scalable, future works will be devoted to optimize the value of the parameters related to the size of the histogram (number of bins) and the Radon transform (number of orientations).

REFERENCES

Arafat, S. Y., Saleem, M., and Hussain, S. A. (2009). Comparative analysis of invariant schemes for logo classification. *International Conference on Emerging Technologies*, pages 256–261.

Chen, Q.-S., Defrise, M., and Deconinck, F. (1994). Symmetric phase-only matched filtering of Fourier-Mellin transforms for image registration and recognition. *IEEE Trans. Pattern Anal. Mach. Intell.*, 16(12):1156–1168.

D., K. C. (1975). The phase correlation image alignment methed. *Proc. Int. Conference Cybernetics Society*, pages 163–165.

Davis, J. and Goadrich, M. (2006). The relationship between precision-recall and roc curves. In *Proceedings of the 23rd international conference on Machine learning*, ICML '06, pages 233–240, New York, NY, USA. ACM.

Deans, S. R. (1993). *The Radon Transform and Some of Its Applications*. Krieger Publishing Company.

Hasegawa, M. and Tabbone, S. (2012). Affine invariant shape matching using Radon transform and dynamic time warping distance. In *ACM Symposium On Applied Computing (ACM SAC), Trento*.

Liang, J., Doermann, D., and Li, H. (2005). Camera–based analysis of text and documents: a survey. *International Journal on Document Analysis and Recognition*, 7(2 – 3):83 – 104.

Lowe, D. G. (2004). Distinctive image features from scale-invariant keypoints. *International Journal of Computer Vision*, 60(2):91–110.

Morel, J.-M. and Yu, G. (2009). ASIFT: A new framework for fully affine invariant image comparison. *SIAM J. Imaging Sciences*, 2(2):438–469.

Ouyang, Z., Feng, J., Su, F., and Cai, A. (2006). Fingerprint matching with rotation-descriptor texture features. In *ICPR (4)*, pages 417–420. IEEE Computer Society.

Santosh, K. C., Lamiroy, B., and Wendling, L. (2011). DTW for matching Radon features: A pattern recognition and retrieval method. In *ACIVS*, pages 249–260.

Tabbone, S., Terrades, O. R., and Barrat, S. (2008). Histogram of Radon transform. a useful descriptor for shape retrieval. In *ICPR*, pages 1–4. IEEE.

Tabbone, S., Wendling, L., and Salmon, J.-P. (2006). A new shape descriptor defined on the Radon transform. *Computer Vision and Image Understanding*, 102(1):42–51.

Tillmann, C., Vogel, S., Ney, H., Zubiaga, A., and Sawaf, H. (1997). Accelerated dp based search for statistical translation. In Kokkinakis, G., Fakotakis, N., and Dermatas, E., editors, *EUROSPEECH*. ISCA.

Yuyama, J. and Mitsuhashi, W. (2008). Shape invariant recognition of polygonal road signs by deforming reference templates. *ICSPCS*, pages 1–6.

Zhang, D. and Lu, G. (2002). Shape-based image retrieval using generic Fourier descriptor. *Sig. Proc.: Image Comm.*, 17(10):825–848.